[9] F. Axisa, Y. Avignon, M. J. Martres, M. Pick, and P. Simon, "Solar coronal streamers observed at 169 MHz with the Nançay E-W radioheliograph," *Solar Phys.*, vol. 19, pp. 110–127, 1971.
[10] E. N. Parker, *Interplanetary Dynamical Processes*. New York: Interscience, 1963.
[11] R. P. Lin and K. A. Anderson, "Electrons ≥ 40-keV and protons ≥ 500 keV of solar origin," *Solar Phys.*, vol. 1, pp. 446–464, 1967.
[12] D. A. Gurnett and R. A. Anderson, "Plasma wave electric fields in the solar wind–Initial results from Helios 1," *J. Geophys. Res.*, vol. 82, pp. 632–650, 1977.
[13] D. F. Smith, "Type III radiobursts and their interpretation," *Space Sc. Rev.*, vol. 16, pp. 91–144, 1974.
[14] J. L. Steinberg, M. Aubier-Giraud, Y. Leblanc, and A. Boischot, "Coronal scattering, absorption and refraction of solar radio bursts," *Astron. Astrophys.*, vol. 10, pp. 362–376, 1971.
[15] J. L. Steinberg, "Coronal scattering of radiobursts at hectometer and kilometer wavelengths," *Astron. Astrophys.*, vol. 18, pp. 383–389, 1972.
[16] J. R. Jokipii, "Turbulence and scintillations in the interplanetary plasma," *Ann. Rev. Astron. Astrophys.*, vol. 11, pp. 1–28, 1973.
[17] C. Caroubalos, M. Aubier, Y. Leblanc, and J. L. Steinberg, "Transfer characteristics of solar radiation in a scattering corona," *Astron. Astrophys.*, vol. 16, pp. 374–378, 1972.
[18] C. Caroubalos, M. Poquerusse, and J. L. Steinberg, "The directivity of type III bursts," *Astron. Astrophys.*, vol. 32, pp. 255–267, 1974.
[19] R. R. Weber, R. J. Fitzenreiter, J. C. Novaco, and J. Fainberg," Interplanetary baseline observations of type III solar bursts," vol. 54, pp. 431–439, *Solar Phys.*, 1977.
[20] J. Fainberg, L. G. Evans, and R. G. Stone, "Radio tracking of solar energetic particles through interplanetary space," *Science*, vol. 178, pp. 743–745, 1972.
[21] P. J. Kellogg, "Tracking of kilometric wavelengths type III solar bursts in elevation and elongation and apparent source size," *Solar Phys.*, vol. 46, pp. 449–458, 1976.
[22] J. L. Steinberg, "Solar stereoradioastronomy," in "Study of travelling interplanetary phenomena," *Proc. L. D. de Feiter Memorial Symp.*, M. A. Shea, D. F. Smart, S. T. Wu, Ed. Dordrecht: D. Reidel, 1978, pp. 65–80.
[23] R. J. Fitzenreiter, J. Fainberg, R. R. Weber, H. Alvarez, F. T. Haddock, and W. H. Potter, "Radio observations of interplanetary magnetic field structures out of the ecliptic," *Solar Phys.*, vol. 52, pp. 477–484, 1977.

A Cosmic Ray Isotope Spectrometer

W. E. ALTHOUSE, A. C. CUMMINGS, T. L. GARRARD, R. A. MEWALDT, E. C. STONE, AND R. E. VOGT

Abstract–**We describe a new instrument to be flown on ISEE-C which is optimized to measure the isotopic composition of solar and galactic cosmic rays with ~5 to ~250 MeV/nucleon. A mass resolution of ≲0.3 AMU should be achieved for all elements with charge $Z \leq 30$.**

I. Introduction

THE Heavy Isotope Spectrometer Telescope (HIST) is designed to measure the isotopic composition and energy spectra of solar, galactic, and interplanetary cosmic ray nuclei for the elements Li through Ni in the energy range from ~5 to ~250 MeV/nucleon. The results of these measurements are important to studies of the isotopic constitution of solar matter and galactic cosmic ray sources, the study of nucleosynthesis processes, studies of particle acceleration, and studies of the life history of cosmic rays in the galaxy.

The HIST instrument consists of a telescope of solid-state detectors and associated signal processing electronics. Resolution of cosmic ray isotopes in HIST is accomplished by a refinement of the standard technique of measuring the particle energy loss ΔE in a detector of thickness L_0 and its residual energy loss E' in a following detector. For example, a particle of mass M, charge Z, and kinetic energy E has a range approximated by

$$R = k \frac{M}{Z^2} \left(\frac{E}{M}\right)^a. \tag{1}$$

Combining this with a similar equation for the range R–L of the particle after traversing a pathlength L, we find

$$M = \left[\frac{k(E^a - E'^a)}{LZ^2}\right]^{1/(a-1)} \tag{2}$$

Isotope resolution, then, depends on precise measurement of the energy losses ΔE and E', the pathlength L (derived from L_0 and the angle of incidence), and an accurate range-energy relation. The HIST detector system and electronics have been designed to optimize mass resolution within power and weight limitations.

II. Instrument Description

A schematic of the HIST telescope is shown in Fig. 1 and summarized in Table I. A unique feature of HIST is the position-sensitive detectors, M1 and M2, which allow the determination of the trajectory of the particle. M1 and M2 are 50-μm-thick surface barrier devices with a matrix of strips forming an x-y hodoscope in place of the conventional con-

Manuscript received April 3, 1978. This work was supported in part by NASA Contract NAS5-20721 and Grant NGR 05-002-160.

The authors are with California Institute of Technology, Pasadena, CA 91125.

0018-9413/78/0700-0204$00.75 © 1978 IEEE

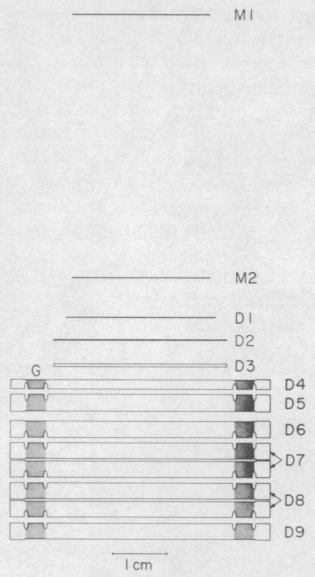

Fig. 1. Schematic of the HIST telescope.

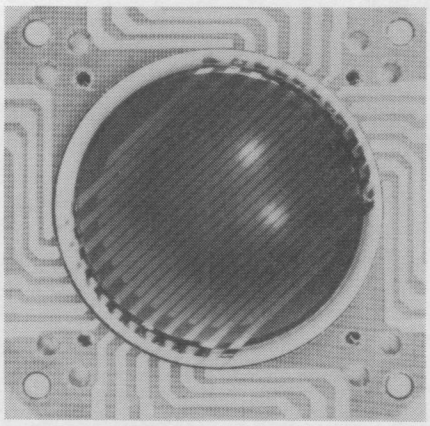

Fig. 2. Photo of a matrix detector.

TABLE I
HIST TELESCOPE CHARACTERISTICS

Det	Thick (μm)	Area (mm^2)	Discr Thresh (MeV)	ADC Thresh (MeV)	ADC Full Scl (GeV)	Aω (cm^2 sr)	Pulse Heights Telemetered
M1	50	505	0.30	0.46	0.49	-	-
M2	50	505	0.30	0.46	0.49	0.32	M1,M2
D1	90	600	0.19	0.54	0.92	0.82	M1,M2,D1
D2	150	800	-	0.71	1.2	0.82	M1,M2,D1,D2
D3	500	800	-	1.46	2.5	0.78	M1,M2,D1,D2,D3
D4	1700	920	-	2.76	4.7	0.74	M1,D1,D2,D3,D4
D5	3000	920	-	3.64	6.2	0.72	M1,D2,D3,D4,D5
D6	3000	920	-	3.64	6.2	0.65	M1,D3,D4,D5,D6
D7	6000	920	-	5.41	9.2	0.58	M1,D4,D5,D6,D7
D8	6000	920	-	5.41	9.2	0.50	M1,D5,D6,D7,D8
D9	3000	920	0.19	-	-	0.43	M1,D5,D6,D7,D8

tinuous evaporated metallic contacts (Fig. 2). There are 24 parallel "x" strips on the Al side, and, orthogonal to these, 24 "y" strips on the Au side. The strips are spaced at 1-mm intervals. Each strip of M1 or M2 is connected to a charge-sensitive preamplifier, shaping amplifier, and threshold discriminator. In addition, signals from the Al strips are summed and digitized by a single 4095-channel ADC in a manner which prevents summing noise from strips which have no signal.

TABLE II
HIST EVENT TYPES

Coincidence Requirement	Description
$M1X \cdot M1Y \cdot M2X \cdot M2Y \cdot Z3 \cdot \overline{D9} \cdot \overline{G2}$	Stopping, $Z \geq 3$
$M1X \cdot M1Y \cdot M2X \cdot M2Y \cdot \overline{Z3} \cdot \overline{D9} \cdot \overline{G1}$	Stopping, $Z < 3$
$M1X \cdot M1Y \cdot M2X \cdot M2Y \cdot D9 \cdot \overline{G2}$	Penetrating, $Z \geq 2$

M1X = logical OR of all M1X strip discriminators
Z3 = 1 for stopping particles with $Z \geq 3$
= 0 otherwise (computed from ADC pulse heights)

Detectors D1, D2, and D3 are conventional surface-barrier detectors, while D4 to D9 are double-grooved Li-drifted detectors [1] with a central area for measuring energy loss and an annular guard (G) used as an anticoincidence shield. Detectors D1, D2, D3, and the centers of D4 through D8 are each direct coupled to separate charge-sensitive preamplifiers, shaping amplifiers, and 4095-channel ADC's. The center of D9 and the guard regions of D4 through D9 are each connected to preamplifiers, shaping amplifiers, and discriminators. Each guard signal channel has two discriminators; G1 is sensitive to minimum ionizing particles while G2 will trigger only on nuclei with more than 5-MeV energy loss.

For particles which stop in detectors M2 through D8 (range 0 through 8), the residual energy E' is measured in the stopping detector and the energy loss ΔE is measured in up to four preceding detectors (see Table I). Highest priority is given to particles with $Z \geqslant 3$; a rotating priority system assures that each range is equally represented in telemetry. For particles which penetrate D9, the energy loss ΔE is measured in D5 through D8; these particles and stopping particles with $Z < 3$ are given lower telemetry priority. The requirements for these event types are summarized in Table II.

Because the telemetry rate is insufficient to transmit every event, rate accumulators are used to count events during 64-s intervals. Instrument live time and stopping $Z \geqslant 3$ events are counted separately in eight directional sectors of spacecraft rotation. Other physical and engineering parameters are also accumulated. These data are used to normalize particle fluxes and monitor instrument health.

Several key features contribute to the performance required to realize the goals of HIST. Except for primary shaping time constants, all circuitry is direct coupled to prevent distortion due to baseline shifts under varying count-rate conditions. A normally open linear gate configuration eliminates delay lines, which often dominate ADC stability and linearity. The linear gate itself operates on a current signal, eliminating offset and transient uncertainties. At the detector input, the ADC has a dynamic range (full scale: ADC threshold) of 1700:1, gain uncertainty due to temperature of ±20 ppm/°C, offset uncertainty of ±0.003 channel/°C, and nonlinearity less than ±1 channel (±0.025 percent of full scale) over the top 99.9 percent of dynamic range. Independent, parallel analog signal processing ensures that this performance is attained for each detector and provides system redundancy as well.

HIST contains 109 preamplifiers, 122 shaping amplifiers, 106 discriminators, 10 4095-channel ADC's, 475 integrated circuits, and associated electronics. The completed HIST instrument weighs 6.5 kg and uses 7 W in a single 12 600-cm^3

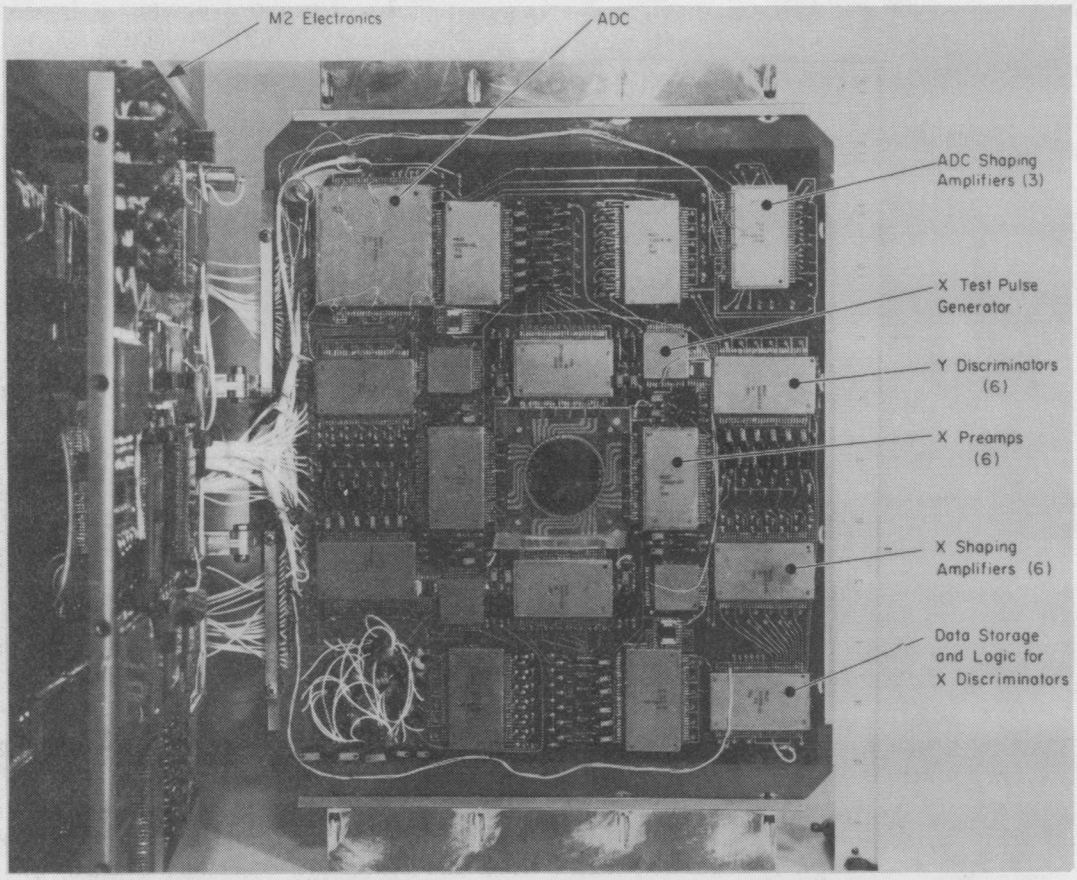

Fig. 3. Photo of the "x" side of the M1 signal processor, folded open. To the left is the "y" side of the M2 signal processor. Six high-precision charge-sensitive preamplifiers are contained in each of the four 2.5 cm × 4.3 cm packages near the center. The remaining hybrids have similar density; for example, the 5 cm × 5 cm ADC hybrid contains 39 discrete transistors, 36 diodes, 48 capacitors, 71 resistors, and 10 integrated circuits.

package. Packaging HIST within the size and mass constraints was accomplished by using custom, thin-film, chip-and-wire hybrid circuitry on planar multilayer printed circuit boards. Fig. 3 demonstrates the high density obtained.

III. Mass Resolution, Calibration, and Expected Response of HIST

The design of HIST reflects the evaluation and optimization of all parameters affecting the mass resolution σ_m. Statistical uncertainties, principally fluctuations in the ΔE measurement, have been minimized by making up to four separate measurements of ΔE. Detectors of graduated thicknesses are used to make this contribution essentially constant over a wide dynamic range in incident particle energy. Systematic effects, mainly uncertainties in knowledge of the pathlength L of the ΔE measurement, have been reduced to the point where the statistical effects dominate. The angular information provided by the matrix detectors reduces the rms uncertainty in L by a factor of ~20, compared to a similar telescope with no position sensing. The trajectory information is also essential in correcting for thickness and charge collection nonuniformities in the ΔE detectors. We have mapped the response of individual detectors to ~0.1 percent using beams of relativistic ^{40}Ar and low-energy protons; one such map is shown in Fig. 4. Electronic contributions to σ_m are negligible. Detailed evaluation shows that HIST should achieve an rms resolution of $\sigma_m \lesssim 0.3$ AMU for all nuclei with $Z \leqslant 30$.

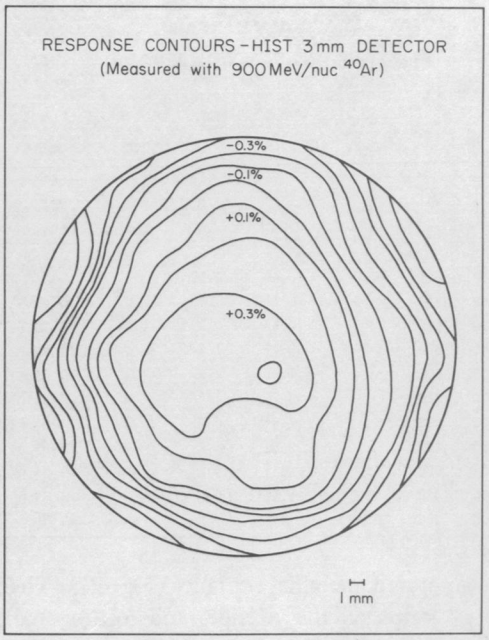

Fig. 4. Detector response contours.

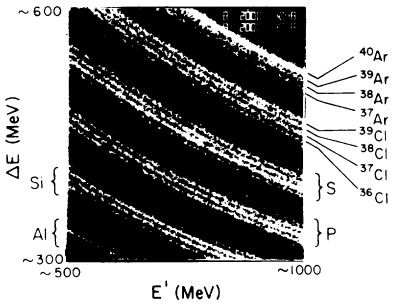

Fig. 5. Raw calibration data showing isotope tracks.

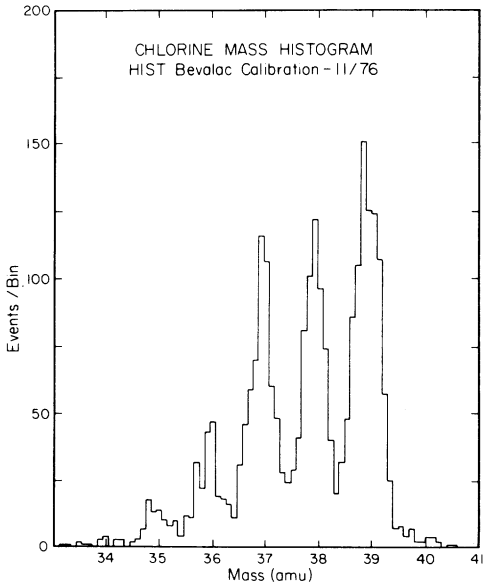

Fig. 6. Mass histogram of Cl calibration data.

TABLE III
EXPECTED EVENT RATES FOR HIST

Element	Energy Interval (MeV/nuc)	Galactic Particles (Events/year)*	Solar Particles (Events/flare)**
He	2.3 - 67	∿ 6300	∿ 2×10^4
O	4.7 - 147	∿ 660	∿ 3×10^4
Ne	5.1 - 168	∿ 160	∿ 4500
Ca	6.4 - 252	∿ 45	∿ 175
Fe	6.2 - 282	∿ 185	∿ 3900

* Normalized to 1967-68 fluxes (2)
** Based on 7/3/74 flare (3)

Because present knowledge of range-energy relations for heavy ions is inadequate, HIST has been exposed to beams of ^{40}Ar and ^{56}Fe at the Bevalac in order to calibrate directly the individual isotope "tracks." Fig. 5 shows an example of such tracks in a ΔE versus E' plot of raw data from D3 and D4 for isotopes of ~50 MeV/nucleon Al through Ar nuclei. In Fig. 6, events from the Cl isotope tracks in Fig. 5 have been converted to a mass histogram, using a technique based on (2) to compute a mass for each event. At least 5 isotopes (^{35}Cl to ^{39}Cl) are clearly visible. The observed resolution of $\sigma_m \simeq$ 0.22 amu will be further improved when the ΔE outputs from D1 and D2 are included in the mass determination.

The energy range covered by HIST for a number of elements is shown in Table III, along with estimates of expected event rates for solar and galactic cosmic ray nuclei. In addition, HIST will be sensitive to low-energy interplanetary particles, including the low-energy ($\lesssim$ 30-MeV/nucleon) anomalous component consisting of He, N, O, Ne, and possibly Ar.

ACKNOWLEDGMENT

Significant contributions to the implementation of the HIST experiment were made by the following organizations and individuals: MDH, Inc., in particular T. Harrington, Dr. J. H. Marshall, and C. Tulga, who designed the electronics and developed the hybrid circuits; J. Jodele was responsible for packaging and mechanical design; Time Zero Laboratories of Ball Brothers Research Corp. was responsible for instrument fabrication under D. Snyder; Halex, Inc. built the custom hybrid circuits; ORTEC, Inc. built the surface-barrier and matrix detectors; Kevex, Inc. furnished the Li-drifted detectors; the Bevalac staff and the Heckman/Greiner group at Lawrence Berkeley Laboratory made possible the ^{40}Ar and ^{56}Fe calibrations; the Kellogg Tandem Lab and the business staff at Caltech provided valuable support; and the staff and students of Caltech's Space Radiation Laboratory, particularly B. Gauld, N. Hickey, M. Smith, and J. Spalding, made many essential contributions. We also thank the ISEE Project Office at GSFC for their patience and support and G. Chapman of ONR for his valuable advice.

REFERENCES

[1] E. C. Stone, R. E. Vogt, F. B. McDonald, B. J. Teegarden, J. H. Trainor, J. R. Jokipii, and W. R. Webber, "Cosmic ray investigation for the Voyager missions: Energetic particle phenomena in the outer heliosphere–and beyond," *Space Sci. Rev.*, vol. 21, pp. 355-376, 1977.

[2] M. Garcia-Munoz, G. M. Mason, and J. A. Simpson, "The abundances of galactic cosmic-ray carbon, nitrogen, and oxygen and their astrophysical implications," *Astrophys. J.*, vol. 184, pp. 967-994, 1973.

[3] R. E. McGuire, T. T. von Rosenvinge, and F. B. McDonald, "Spectra and composition 2-40 MeV/nucleon of ions Z = 2-28 in solar cosmic ray events," in *Conf. Papers*, 15th Int. Cosmic Ray Conf., Plovdiv, Bulgaria, vol. 5, pp. 54-59, 1977.